J. Phys. Chem. B **2006,** *110,* 24869−24875

Raman Scattering in Crystalline Oligothiophenes: A Comparison between Density Functional Theory and Bond Polarizability Model

P. Hermet,*,[†] N. Izard,[‡] A. Rahmani,[§] and Ph. Ghosez[†]

Département de Physique, Université de Liège, B-5, 4000 Sart-Tilman, Belgium, Laboratoire des Colloïdes, Verres et Nanomatériaux (UMR CNRS 5587), Université Montpellier II, 34095 Montpellier Cédex 5, France, and Département de Physique, Université MY Ismail, 50000 Meknès, Morocco

Received: July 24, 2006; In Final Form: September 20, 2006

Raman intensity of intramolecular and lattice modes of crystalline α-bithiophene (α-2T) are investigated within density functional theory using a nonlinear response formalism. First, comparison between the calculated Raman spectrum and the experimental data allows the assignment of the main Raman lines over the whole frequency range. Then, a bond polarizability (BP) model, limited to first neighbors, is built. We show that, although the BP model cannot reproduce the changes of dielectric susceptibility under individual atomic displacements, it is accurate enough to reproduce the profile of the unpolarized nonresonant Raman spectrum of α-2T powder. Finally, the BP model, fitted on our first-principles results on α-2T, is applied with success to the α-quaterthiophene polymorph phases and α-sexithiophene, demonstrating on practical examples that first-principles and BP approaches are powerful complementary tools to calculate the nonresonant Raman spectrum of α-2T and make reasonable predictions on larger oligothiophenes.

1. Introduction

Oligothiophenes and their derivatives are currently among the most studied π-conjugated organic materials because of their environmental stability, easy functionalization, and several potential technological applications in electronics and optoelectronics.[1−4] In these materials, the electronic and optoelectronic properties depend on the extent of the overlap between the p_z orbitals of the carbon atoms at the α,α′-positions (see Figure 1), which is either promoted or hindered by the low-frequency dynamics via the internal rotation around the single bonds between adjacent thiophene rings.

Raman spectroscopy is a powerful tool for investigating the molecular structure and electronic interactions of π-conjugated oligomers.[5] Nevertheless, due to their relative complexity, the experimental Raman spectra in the crystalline phases of these materials cannot be fully understood without the additional support of theoretical calculations. Density functional theory (DFT)[6,7] has proved to be successful in the calculation of the lattice dynamics of oligothiophenes by using both the isolated molecules[8] and the crystalline phase[9−11] models. However, while DFT is routinely used for the determination of vibrational frequencies, its application to Raman activities is less frequently applied to crystalline phases and is still challenging in oligothiophenes (or in π-conjugated oligomers), mainly because of the very high computational effort and accuracy required in the calculation of the Raman susceptibility tensors. In the literature, calculations of the Raman spectra in oligothiophenes have been restricted to isolated molecule models, using either empiric force field,[12] semiempirical methods,[13,14] or first-principles methods.[15,16] Within these models, the assignments of the Raman phonon modes are therefore limited to intramolecular vibrations, so that the low-frequency assignments (i.e., below 500 cm^{-1}), where low-frequency molecular and lattice modes mix, are questionable.

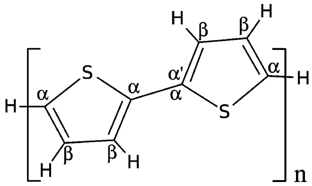

Figure 1. Atom labels in α-2T ($n = 1$), α-4T ($n = 2$), and α-6T ($n = 3$).

In this paper, we calculate the position and intensity of the Raman lines of a prototype crystalline oligothiophene: the α-bithiophene (α-2T). First, these quantities are determined within DFT, taking advantage of a recent implementation based on the nonlinear response formalism and the $(2n + 1)$ theorem,[17,18] and an assignment of the main Raman lines is proposed over the whole frequency range. Then, taking our DFT results as reference, we build a bond polarizability (BP) model[19,20] limited to first neighbors. Such a simple model, which was never previously applied to π-conjugated systems with rings, constitutes an interesting alternative to first-principles methods to compute, at low computational efforts, the nonresonant Raman intensities of crystalline phases of oligothiophenes. The successes and the limitations of this model are discussed, as well as the transferability of the BP parameters to longer oligothiophenes.

This paper is organized as follows. In the next section, we give the experimental conditions in the acquisition of Raman spectra of oligothiophenes. In section 3, we describe the model used to compute the nonresonant Raman scattering spectra of oligothiophenes. In section 4, the DFT-calculated unpolarized nonresonant Raman spectrum of α-2T polycrystalline powder is compared to the experimental one, and a vibrational assignment at the Γ-point of the Brillouin zone is proposed for the

---

* Corresponding author. E-mail: Patrick.Hermet@ulg.ac.be.
[†] Université de Liège.
[‡] Université Montpellier II.
[§] Université MY Ismail.

10.1021/jp064700n CCC: $33.50

main lines of α-2T over the whole frequency range. A discussion about the validity of the BP model in oligothiophenes and the methods used for calculating the BP parameters are given in section 5, whereas section 6 investigates the transferability of the BP parameters in the α-quaterthiophene (α-4T) polymorph phases and α-sexithiophene (α-6T). Finally, our results are summarized in section 7.

2. Experimental Setup

Macro-Raman experiments, for both α-2T and α-4T (commercial samples obtained from Sigma Aldrich Inc.), were performed on a FT Bruker RFS100 spectrometer using the fundamental line of a Nd:YAG continuous laser at 1064 nm (1.16 eV) as incident excitation. Since the gap in non-substituted α-2T is 3.68 eV,[21,22] we can reasonably consider a nonresonant Raman process. A notch filter is used to remove the elastic scattering. Unpolarized Raman spectra were recorded on powder samples in the 80−3500 cm^{-1} range at room temperature. Acquisition time was 3 h, and the resolution was 4 cm^{-1}. To avoid sample heating, the laser power was limited to 10 mW. The low energy of the incident laser line did not trigger sample photoluminescence, which usually overlaps the Raman responses for visible incident excitations.

3. Theory of Raman Scattering

The scattering efficiency in a given direction, with a frequency between ω_d and $\omega_d + d\omega_d$, and within a solid angle $d\Omega$, is given for a Stokes process by[23]

$$\frac{d^2S}{d\Omega d\omega_d} = \frac{\omega_d^4}{16\pi^2c^4}[B(\omega)+1]\hbar \mathbf{v}_i \mathbf{v}_k I_{ijkl}(\omega) \mathbf{w}_j \mathbf{w}_l \tag{1}$$

where $\omega = \omega_0 - \omega_d$, and

$$I_{ijkl}(\omega) = \sum_m a_{ij}{}^*(m) a_{kl}(m) \frac{1}{2\omega_m}[\delta(\omega - \omega_m) - \delta(\omega + \omega_m)] \tag{2}$$

In these equations, (i,j,k,l) indices denote the Cartesian components, the asterisk symbolizes the complex conjugation, c is the speed of light in the medium, $\hbar$ is the reduced Planck constant, ω_0 (respectively ω_d) is the frequency of incident (respectively scattered) light, $\mathbf{v}$ (respectively $\mathbf{w}$) is the polarization unit vector of the incident (respectively scattered) light, $B(\omega)$ is the Bose factor, and ω_m is the frequency of the mth zone-center phonon mode. The Raman susceptibility tensor is defined as

$$a_{ij}(m) = \sqrt{\Omega_0}\sum_{\kappa\gamma} \pi^{\kappa}_{ij,\gamma}\, u_m(\kappa\gamma) \tag{3}$$

where the sum runs over all atoms κ and space directions γ, Ω_0 is the unit cell volume, $u_m(\kappa\gamma)$ is the $(\kappa\gamma)$ component of the mth phonon eigendisplacement vector, and $\tilde{\pi}$ is a third-rank tensor describing the changes of optical dielectric susceptibility ($\tilde{\chi}^{\infty}$) induced by individual atomic displacements. This latter quantity is defined as

$$\pi^{\kappa}_{\mathrm{ij},\gamma} = \frac{\partial \chi^{\infty}_{\mathrm{ij}}}{\partial \tau_{\kappa\gamma}} \tag{4}$$

where $\tau_{\kappa\gamma}$ corresponds to the displacement of the κth atom in the direction γ. As long as the phonon frequencies and eigendisplacements are known, $\tilde{\pi}$ is the central quantity to be determined in order to estimate Raman intensities. As it is further discussed in sections 4A and 5A, it can be computed directly from first-principles or estimated within the BP model.

To obtain a relation between the Raman tensors and the scattering intensities for a polycrystalline powder, the Raman tensors must be subject to orthogonal transformations with arbitrary angles, and the results must be averaged over the whole angular space. This is done by evaluating the Raman tensor component for various orientations in space using the Euler's angles.[24] In the following, we assume that the incident and scattered light are polarized parallel to the axes of the laboratory frame, so that we have $j = l$ and $i = k$ in eqs 1 and 2. In addition, for all the calculated spectra shown in this paper, the Raman line shape is assumed to be Lorentzian and the line width is fixed at 4 cm^{-1}, except for the α-6T where the line width is fixed at 12 cm^{-1}.

4. Raman Scattering Intensities in α-2T from First-Principles

A. Computational Details. Our first-principles study of α-2T was performed within DFT, as implemented in the ABINIT package.[25] Calculations on α-2T were performed at the experimental volume and lattice parameters.[26] Relaxations of internal atomic positions were done by using the Broyden−Fletcher−Goldfarb−Shanno algorithm[27] until the maximum residual force on the atoms was less than 6×10^{-6} Ha/Bohr. The exchange correlation energy functional was evaluated within the local density approximation, using the Perdew−Wang parametrization[28] of Ceperley−Alder homogeneous electron gas data.[29] The all-electron potentials were replaced by norm-conserving pseudopotentials generated according to the Troullier−Martins scheme[30] thanks to a package developed at the Fritz-Haber Institute (Berlin).[31] Hydrogen (1s), sulfur ($3s^2$, $3p^4$) as well as carbon ($2s^2$, $2p^2$)-electrons were considered as valence states in the construction of the pseudopotentials. The electronic wave functions were expanded in plane waves up to a kinetic energy cutoff of 40 Ha. Integrals over the Brillouin zone were approximated by sums over a 4 × 5 × 3 mesh of special k-points according to the Monkhorst−Pack scheme.[32]

The dynamical matrix yielding the phonon frequencies and eigenvectors was obtained within a variational approach to density functional perturbation theory.[33] The derivatives of the dielectric susceptibility with respect to atomic displacements, $\pi^{\kappa}_{ij,\gamma}$ (eq 4), are related to a mixed third-order derivative with respect to two electric fields and one atomic displacement of the field-dependent energy functional, $\mathcal{F} = E - \Omega_0\, \mathcal{E}\cdot\mathcal{P}$, as defined in ref 34, where E is the total energy in zero field and $\mathcal{E}$ (respectively $\mathcal{P}$) are the macroscopic electric field (respectively polarization):

$$\pi^{\kappa}_{ij,\gamma} = -\frac{1}{\Omega_0}\frac{\partial^3 \mathcal{F}}{\partial \mathcal{E}_i\, \partial \mathcal{E}_j\, \partial \tau_{\kappa\gamma}} \tag{5}$$

These derivatives are evaluated at the equilibrium atomic positions and under the condition of zero electric field (respectively displacement field) for transverse (respectively longitudinal) optic phonon modes. They were obtained within a nonlinear response formalism, taking advantage of the $(2n+1)$ theorem as described in ref 17. For this latter calculation, the perturbation expansion after discretization (PEAD) formulation was used. Convergence of Raman response with respect to the basis set size and to the Brillouin zone sampling was tested using a cutoff of 50 Ha on plane-wave energy and a 5 × 6 ×

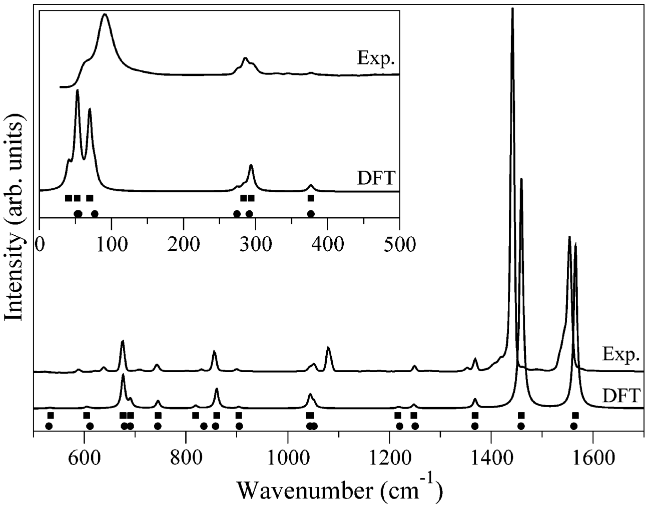

Figure 2. Comparison between the unpolarized experimental nonresonant Raman spectra of α-2T polycrystalline powder and the DFT-calculated one. The calculated spectrum has been normalized on the experimental line centered at 855 cm^{-1} for the presentation. Inset: Low-frequency domain of the unpolarized nonresonant Raman spectrum of α-2T. The position of the A_g and B_g modes are symbolized by squares and circles respectively in the bottom of these figures.

4 *k*-point grid, leading to a maximum variation of 3 cm^{-1} on the Raman frequencies and 5% on Raman susceptibilities calculations.

B. Vibrational Dynamics. α-2T crystallizes in the $P2_1/c$ ($C_{2h}{}^5$) monoclinic space group with two molecules per unit cell.[26] The eigenmodes of the dynamical matrix transform according to the irreducible representation (A_u, A_g, B_u, and B_g) of the point group symmetry C_{2h}, which are non-degenerates. In Raman spectroscopy, only modes that transform under symmetry operations as a quadratic form are active. Thus, only the A_g or B_g modes are Raman active.

Figure 2 compares the unpolarized nonresonant Raman spectra of α-2T polycrystalline powder calculated within DFT and measured experimentally at room temperature in the 0−1700 cm^{-1} range. Positions of the A_g and B_g modes are also reported in this figure. A single scale factor was applied to compare the intensity of the experimental and calculated Raman spectra. We observe that the frequency positions, as well as the calculated relative spectral intensities, of the Raman active modes are in good agreement with the experimental ones. This demonstrates respectively the accuracy of the calculations of the dynamical matrix and of the Raman susceptibility tensors. This close agreement between theory and experiment allows to propose convincing mode assignments for the most intense experimental Raman lines.

Let us first consider the experimental range 500−1400 cm^{-1}. This frequency range is dominated by two features centered at 676 and 855 cm^{-1}, three weak lines centered at 742, 1250, and 1368 cm^{-1}, and one doublet around 1075 cm^{-1}. Frequency position and relative intensity of these experimental lines are correctly simulated, except for the experimental doublet centered around 1075 cm^{-1}. Indeed, although the experimental doublet splitting is correctly reproduced by the calculation with two lines at 1044 and 1052 cm^{-1}, the 3% discrepancy with respect to the experiment in the calculated frequency position of this latter line leads to an underestimation of the calculated doublet splitting. Analyzing the corresponding eigenvectors, the experimental lines previously enumerated are assigned respectively to a $\delta(C_\alpha - S - C_\alpha) + \gamma(C - H)$ [676 cm^{-1}], $\nu(C_\alpha - S) + \delta(C - H)$ [855 cm^{-1}], $\nu(C_\alpha - S) + \delta(C_\alpha = C_\beta - C_\beta)$ [742 cm^{-1}], $\delta(C_\alpha - C_\alpha - C_\beta) + \delta(C - H)$ [1250 cm^{-1}], and $\delta(C_\beta - C_\alpha - S) + \nu(C_\beta - C_\beta)$ [1368 cm^{-1}] (see Figure 1 for the atom labels, and[35] for the nomenclature used). The two experimental lines centered at 1050 and 1080 cm^{-1}, constitutives of the doublet, are assigned to $\delta(S - C_\alpha = C_\beta) + \delta(C - H)$ vibrations.

The well-known experimental range 1400−1700 cm^{-1} is dominated by two strong lines centered at 1442 and 1554 cm^{-1}, assigned to $\nu_s(C_\alpha = C_\beta) + \delta(C_\alpha - S - C_\alpha)$ and $\nu_{as}(C_\alpha = C_\beta) + \delta(C_\alpha - S - C_\alpha)$ vibrations, respectively. These two lines are in good agreement with the calculated ones, both in frequency positions and in relative intensities. It is interesting to note that in most cases the Raman lines in the 500−1700 cm^{-1} range are a combination of a A_g symmetry mode and a B_g symmetry mode (see Figure 2). In addition, the assignments given in the 500−1700 cm^{-1} range are both in agreement and complementary to those obtained either theoretically using a α-2T isolated molecule model,[12,15] or experimentally by filiation with Raman spectra of longer oligothiophenes.[36−38]

Let us focus now on the experimental range 0−500 cm^{-1} (inset of Figure 2). For frequencies below 80 cm^{-1}, no experimental Raman data were found in the literature. Nevertheless, four Raman modes (two A_g symmetry modes centered at 40 and 52 cm^{-1} and two B_g symmetry modes centered at 53 and 54 cm^{-1}) are predicted by the calculation. These lines are assigned to a ring torsion for the A_g modes, whereas the B_g modes are assigned to an antisymmetric butterfly and $\delta(C_\alpha - S - C_\alpha) + \delta(C - H)$ modes, respectively. In the 80−300 cm^{-1} range, the experimental spectrum is dominated by two broad lines centered around 90 and 300 cm^{-1}. The asymmetric line shape of the experimental lowest frequency feature is due to the cut of the Notch filter used to remove the elastic scattering. Nevertheless, the presence of experimental Raman modes around 90 cm^{-1} is obvious. In agreement with this observation, two Raman modes of A_g and B_g symmetry, respectively centered at 70 and 77 cm^{-1}, are predicted by the calculation and assigned both to a ring torsion. Next, around 300 cm^{-1}, the weak multipeak structure observed in the experimental spectrum corresponds to two A_g symmetry modes calculated at 283 and 294 cm^{-1}, and two B_g symmetry modes calculated at 274 and 291 cm^{-1}. These modes are assigned to a ring torsion of thiophene moieties for the lines at 274 and 283 cm^{-1} and to a $S - C_\alpha - C_\alpha - S$ scissor for the lines at 291 and 294 cm^{-1}. Finally, to the experimental weak line centered at 377 cm^{-1} corresponds two calculated lines of A_g and B_g symmetry centered at the same frequency, and assigned to a $\delta(S - C_\alpha - C_\beta) + \delta(C - H)$ phonon mode.

5. Raman Scattering Intensities in α-2T from BP Model

A. The BP Model. The BP model considers that the optical dielectric susceptibility ($\tilde{\chi}^\infty$) of the crystal can be decomposed into individual contributions, arising only from the polarizability ($\tilde{\alpha}^b$) of bonds b between nearest-neighbor atoms,

$$\chi_{ij}^{\infty} = \frac{1}{\Omega_0}\sum_b \alpha_{ij}^b \qquad (6)$$

and the polarizability of a particular bond b is assumed to be given by the empirical equation[19,20]

$$\alpha_{ij}^b = \frac{1}{3}(\alpha_l + 2\alpha_p)\delta_{ij} + (\alpha_l - \alpha_p)\left(\hat{r}_i\hat{r}_j - \frac{1}{3}\delta_{ij}\right) \qquad (7)$$

TABLE 1: Optimized BP Parameters for the BP/$\tilde{\pi}$ and the BP/Spectrum Models for Each Type of Bond in the α-2T[a]

	BP/$\tilde{\pi}$ model			BP/spectrum model		
	$\bar{\alpha}$	$\bar{\beta}$	$\bar{\gamma}$	$\bar{\alpha}$	$\bar{\beta}$	$\bar{\gamma}$
$C_\alpha - C_\alpha$	−113.7	−183.4	−11.3	−113.6	8.9	17.1
$C_\alpha = C_\beta$	110.2	−15.9	9.5	310.0	88.8	75.5
$C_\beta - C_\beta$	−11.2	−82.7	−10.5	−60.4	−10.2	−7.4
$C_\alpha - S$	78.8	28.8	18.1	153.7	77.8	−63.2
$C_\alpha - H$	48.2	4.3	−3.0	59.6	5.1	−6.1
$C_\beta - H$	31.5	18.7	0.8	59.9	4.6	4.6

[a] The units of BP parameters are given in Bohr^{-1} for $\bar{\alpha}$ and $\bar{\beta}$, except for the $\bar{\gamma}$ parameter, which is undimensioned.

where the indices i and j denote the Cartesian components and $\hat{r}$ is the unit vector along the bond b. The parameters α_l and α_p correspond to the longitudinal and perpendicular bond polarizability, respectively. A further assumption of the BP model is that the BP parameters are functions of the bond lengths r only, so that the derivative of the polarizability tensor with respect to the displacement of atom κ in direction γ is given by

$$\frac{\partial \alpha^b_{ij}}{\partial \tau_{\kappa\gamma}} = \frac{1}{3}(2\alpha'_p + \alpha'_l)\delta_{ij}\hat{r}_\gamma + (\alpha'_l - \alpha'_p)\left(\hat{r}_i\hat{r}_j - \frac{1}{3}\delta_{ij}\right)\hat{r}_\gamma + \frac{\alpha_l - \alpha_p}{r}(\delta_{i\gamma}\hat{r}_j + \delta_{j\gamma}\hat{r}_i - 2\hat{r}_i\hat{r}_j\hat{r}_\gamma) \quad (8)$$

where $\alpha'_{l(p)} = (\partial \alpha_{l(p)}/\partial r)|_{r=r_0}$ and r_0 is the equilibrium distance. Within the BP model, the third-order tensor coefficients, $\pi^\kappa_{ij,\gamma}$ (eq 4), are therefore obtained as

$$\pi^\kappa_{ij,\gamma} = \frac{1}{\Omega_0}\sum_b \frac{\partial \alpha^b_{ij}}{\partial \tau_{\kappa\gamma}} \quad (9)$$

In α-2T, six types of bond occur: $C_\alpha - C_\alpha$, $C_\alpha = C_\beta$, $C_\alpha - S$, $C_\beta - C_\beta$, $C_\beta - H$, and $C_\alpha - H$ (see Figure 1). Since the BP model is completely defined by three parameters ($\bar{\alpha} = 2\alpha'_p + \alpha'_l$, $\bar{\beta} = \alpha'_l - \alpha'_p$, and $\bar{\gamma} = \alpha_l - \alpha_p$) for each type of bond, we must consider 18 parameters in the model. In practice, we can determine these 18 parameters by fitting either (i) the third-order tensor coefficients, $\pi^\kappa_{ij,\gamma}$ (eqs 8 and 9), obtained from DFT calculations (BP/$\tilde{\pi}$ model), or (ii) directly the experimental Raman lines through eqs 1−3 (BP/spectrum model). We examine these two methods for obtaining the BP parameters in the next two subsections.

B. The BP/$\tilde{\pi}$ Model. In a first approach, we have determined the 18 BP parameters by using only eqs 8 and 9 and the $\pi^\kappa_{ij,\gamma}$ tensor coefficients obtained previously from our DFT calculations. Since we have 8 atoms in the asymmetric unit cell of crystalline α-2T in general position, and since the polarizability tensor is symmetric, the $\pi^\kappa_{ij,\gamma}$ coefficients have 144 nonzero independent elements. Thus, we must resolve an overdetermined linear system, $\tilde{A}\tilde{X} = \tilde{\pi}$, of 144 independent equations with 18 unknowns in order to determine the BP parameters of α-2T, where $\tilde{A}$ is a 144-by-18 matrix containing the coefficients ($\bar{\alpha}$, $\bar{\beta}$ and $\bar{\gamma}$) for each type of bond and $\tilde{X}$ is the 18-element solution vector. In general, this system has no exact solution, but the linear least-squares problem can be solved. The BP/$\tilde{\pi}$ model parameters reported in Table 1 were obtained by minimizing the Euclidian norm $||\tilde{A}\tilde{X} - \tilde{\pi}||_2$ using a LAPACK subroutine.[39] This minimization gives a mean relative error of 118%. The relative error is however of less than 50% on half of the $\pi^\kappa_{ij,\gamma}$ coefficients. Although such errors are large, it is worth noticing that they are comparable to those previously reported by Umari et al.[40] using a similar approach on α-quartz.

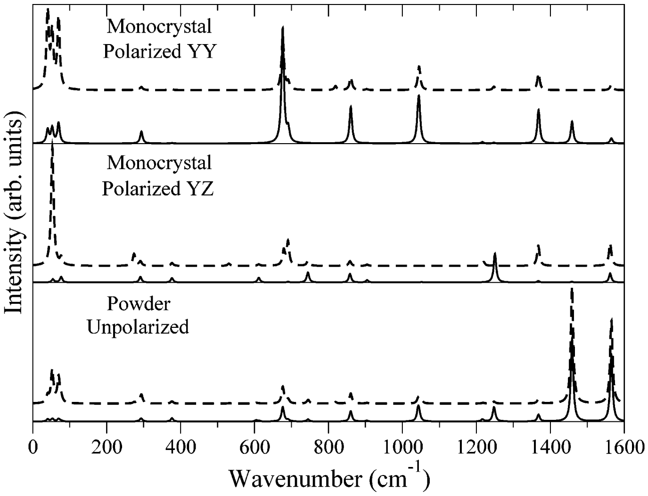

Figure 3. Calculated nonresonant Raman spectra of α-2T from DFT calculations (dashed lines) and BP/$\tilde{\pi}$ model (continuous lines).

The $\tilde{\pi}$ coefficients describe the change of dielectric susceptibility with respect to individual atomic displacements and are the microscopic quantities related to the Raman susceptibilities. The fact that these coefficients cannot be reproduced accurately within the BP model framework demonstrates that this simple model does not strictly apply to α-2T. In other words, the underlying hypothesis that the polarizability of atoms is modulated only by nearest neighbor bonds and that the BP parameters are dependent only on the bond lengths are not perfectly satisfied in α-2T (or more generally in π-conjugated materials), due to the important delocalization of the π-electrons.

Figure 3 compares the nonresonant Raman spectrum of α-2T calculated on polycrystalline powder for an unpolarized configuration, and on monocrystal with a *YY* and *YZ* polarizations, by using the BP/$\tilde{\pi}$ model and the DFT calculations. For a *YY* (*YZ*) polarization, the incoming and the scattered photons have a polarization along *Y* (*Y*) and *Y* (*Z*), respectively. In our rectangular reference system, the X-, Y- and Z-axes are respectively parallel to the *a*-crystal axis, the monoclinic *b*-crystal axis, and in the *ac* plane. For the monoclinic crystal and for the rectangular reference system used, the Raman susceptibility tensors of the A_g and B_g modes have a well-defined form given respectively by[41]

$$\begin{pmatrix} a & & d \\ & b & \\ d & & c \end{pmatrix}$$

and

$$\begin{pmatrix} & e & \\ e & & f \\ & f & \end{pmatrix}$$

As discussed in section 3, the Raman scattering efficiencies can be computed from the projection of the Raman susceptibility tensors on the polarization vectors of the incoming and scattered photons. Thus, with a *YY* (and *YZ*) polarization, the intensity of the A_g (and B_g) Raman lines depends on the element b (and f) of their Raman susceptibility tensors. To compare strictly the Raman intensity differences between the BP/$\tilde{\pi}$ model and the DFT calculation, no scale factor has been applied on the intensity of these spectra.

As expected from the poor description of the $\pi^{\kappa}_{ij,\gamma}$ coefficients, Figure 3 shows that the α-2T Raman intensities calculated with the BP/$\tilde{\pi}$ model on a monocrystal are significantly different from the DFT results. For instance, in the *YY* polarization, the Raman spectrum calculated within the BP/$\tilde{\pi}$ model displays three strong lines centered at 850, 1367 and 1450 cm^{-1}, whereas the spectrum calculated with DFT displays respectively two small lines at 850 and 1367 cm^{-1} and no line at 1450 cm^{-1}. In the same way, in the *YZ* polarization, the spectrum calculated with DFT displays a very strong line centered at 53 cm^{-1}, a strong line centered at 1365 cm^{-1}, and one strong doublet centered around 650 cm^{-1}, whereas the spectrum calculated within the BP/$\tilde{\pi}$ model displays respectively a small and a weak lines in these frequencies, and no doublet around 650 cm^{-1}.

By contrast, in the lowest panel of Figure 3, we observe that both the position and intensities of the Raman lines calculated with the BP/$\tilde{\pi}$ model are much closer to the DFT results for a polycrystalline powder, except for the intensities of the low-frequency lines below 100 cm^{-1} which are underestimated, and the high-frequency lines centered at 1040 and 1247 cm^{-1}, which are lightly overestimated in the BP/$\tilde{\pi}$ spectrum. This means that the average over all orientations of space of Raman tensors used to construct the polycrystalline spectrum compensate to some extent the deficiencies of the BP/$\tilde{\pi}$ model.

So, from these analyses, it appears that although the $\tilde{\pi}$ tensor of individual atoms is not strictly reproduced within the BP model, this model remains accurate enough to reproduce the main features of the unpolarized nonresonant Raman spectrum on α-2T polycrystalline powder.

C. The BP/Spectrum Model. Usually the BP parameters are not fitted at the microscopic level to reproduce the individual $\pi^{\kappa}_{ij,\gamma}$ coefficients but are adjusted to reproduce globally the intensities of the experimental Raman spectrum. Following this much conventional approach, the 18 parameters of the BP model in α-2T are now determined by fitting the 15 main experimental intensities of α-2T Raman spectrum between 200 and 1600 cm^{-1}, which is the frequency range best defined experimentally. As the number of unknowns is larger than the number of Raman lines seen in the experimental spectrum, the solution is not unique and various combination of parameters might provide a similar accuracy on the spectrum. Moreover, following this procedure, the BP parameters are undetermined within a scaling factor because the experimental Raman intensities are only known on a relative scale. In this context, for a direct comparison with the BP/$\tilde{\pi}$ model, we have chosen this scaling factor so that the $\bar{\alpha}(C_\alpha - C_\alpha)$ parameter is normalized to its BP/$\tilde{\pi}$ model value. The three ajustable parameters ($\bar{\alpha}, \bar{\beta}, \bar{\gamma}$) obtained for each type of bond, and after normalization, are given in Table 1.

Figure 4 displays the experimental unpolarized Raman spectrum of α-2T on a polycrystalline powder with those calculated using the BP/$\tilde{\pi}$ and BP/spectrum models in the 0−1700 cm^{-1} range. In the 200−1700 cm^{-1} range, frequency positions of the calculated Raman lines by using the BP/spectrum model are in good agreement with the experimental ones. Calculated relative spectral intensities are also in good agreement with the measured ones, except for the lines below 550 cm^{-1}, which are overestimated in the BP/spectrum model. For frequencies smaller than 200 cm^{-1}, the lines in the α-2T experimental Raman spectrum have not been used to adjust the BP parameters. Nevertheless, similarly to the BP/$\tilde{\pi}$ model, the BP/spectrum model predicts three lines centered at 40, 54, and 69 cm^{-1}.

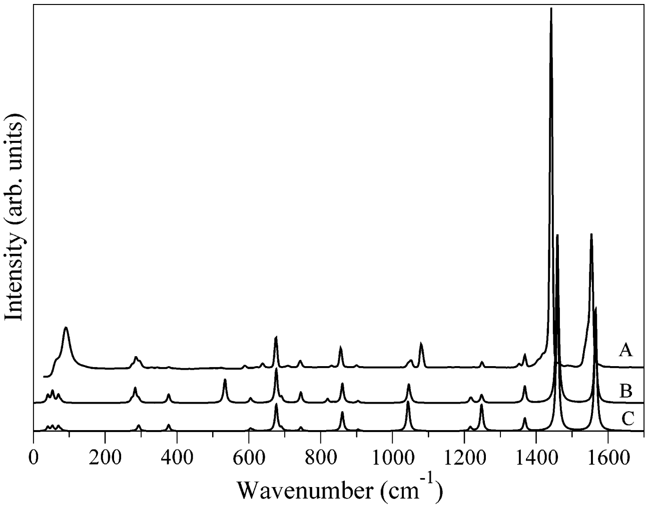

Figure 4. Comparison between the unpolarized experimental (A) nonresonant Raman spectra on α-2T polycrystalline powder and the ones calculated by using the BP/spectrum (B) and BP/$\tilde{\pi}$ (C) models.

It is worth noticing that, in order to obtain the BP/$\tilde{\pi}$ parameters, only the structure of α-2T is relevant while the BP/spectrum parameters are additionally dependent on the experimental conditions (polarized or unpolarized) and the type of sample (powder or monocrystal). In case where the BP parameters are fitted on the experimental spectrum, these parameters will be also influenced by experimental factors such as the line width, the resolution and the temperature. In this respect, the BP/$\tilde{\pi}$ parameters should be a priori more transferable to other configurations or longer oligothiophenes. This is now investigated by applying the two sets of α-2T BP parameters given in Table 1 to the α-4T polymorph phases and α-6T.

6. Transferability of α-2T BP Parameters To Longer Oligothiophenes

A. Raman Intensities in α-4T Polymorph Phases. α-4T crystallizes in the monoclinic space group and packs according to a herringbone structure. However, two polymorph phases have been observed depending on the conditions of crystal growth. Single crystals grown from the vapor phase method (synthesis at low temperature) pack in the $P2_1/c$ ($C_{2h}{}^5$) space group with a number of molecules per unit cell equal to $Z = 4$ (α-4T/LT phase), whereas those grown from the melt (synthesis at high temperature) pack in the $P2_1/a$ ($C_{2h}{}^5$) space group with $Z = 2$ (α-4T/HT phase).[42]

In this section, the frequency position of the Raman lines corresponds to the phonon frequencies previously computed in ref 43 using the implementation of the direct method.[44] Thus, the frequency position of the Raman lines was calculated from the diagonalization of the dynamical matrix obtained by DFT-based methods, whereas the Raman intensities are calculated within the empirical nonresonant BP model by using the two sets of parameters given in Table 1.

Figure 5 compares the experimental unpolarized nonresonant Raman spectrum of α-4T/LT polycrystalline powder with the one calculated using the BP/$\tilde{\pi}$ and the BP/spectrum models in the 0−1600 cm^{-1} range. Positions of Raman active modes calculated by using the BP/$\tilde{\pi}$ model are in good agreement with the position of the main experimental Raman lines. Calculated relative spectral intensities are also in good agreement with the measured ones, except for the intensity of the lines centered around 600 and 1250 cm^{-1}, which are overestimated with respect to the experiment in the calculated Raman spectrum. At the opposite, this agreement is rather poor for the Raman

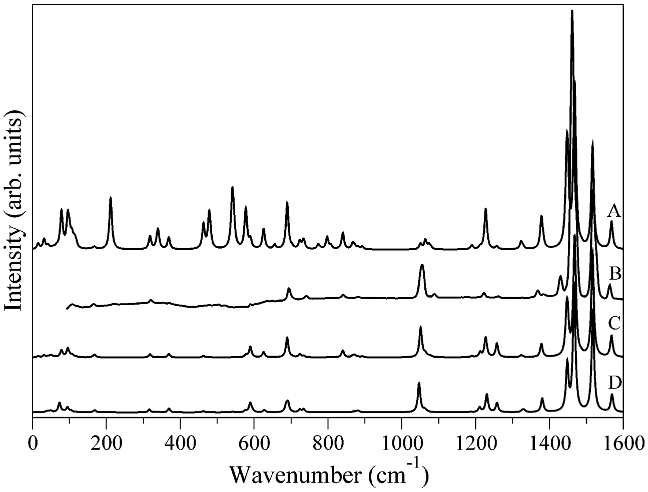

Figure 5. Comparison between the unpolarized experimental nonresonant Raman spectrum on α-4T polycrystalline powder (B) and the ones calculated by using the BP parameters obtained from the BP/spectrum model for the LT phase (A) and the BP/$\tilde{\pi}$ model for the LT (C) and HT (D) phases. The calculated spectra have been normalized on the experimental line centered at 1516 cm^{-1}.

spectrum calculated by using the BP/spectrum model. So, the α-2T BP parameters obtained at a microscopic level from the BP/$\tilde{\pi}$ model are transferable in the case of α-4T, whereas the BP parameters obtained on the experimental data from the BP/spectrum model are not.

To the best of our knowledge, there is no experimental or calculated Raman spectrum of the α-4T/HT phase in the literature. Thus, we have applied the transferability of the BP parameters obtained from our BP/$\tilde{\pi}$ model (i) to predict the Raman spectrum of α-4T/HT phase, and (ii) to investigate the Raman signatures which allow unambiguously the α-4T/HT and α-4T/LT phases to be identified. Figure 5 also compares the calculated unpolarized nonresonant Raman spectra on a polycrystalline powder of α-4T/LT and α-4T/HT phases by using the BP/$\tilde{\pi}$ model with the experimental α-4T/LT spectrum measured at room temperature. For the frequencies higher than 150 cm^{-1}, the calculated α-4T/LT Raman spectrum displays, according to the experimental spectrum, a small line centered at 830 cm^{-1} which is absent in the calculated α-4T/HT spectrum. This line centered at 830 cm^{-1} is therefore a Raman fingerprint of a α-4T/LT phase for the high-frequency range. No significant spectral contribution allows this identification in this frequency range. Since the α-4T polymorph phases differ in the packing of the 4T molecules, some differences in the spectral signatures on the α-4T/HT and α-4T/LT phases should also be located in the low-frequency range, to which the supramolecular arrangement is very sensitive. Indeed, the calculation of the nonresonant Raman spectrum of α-4T/LT predicts two small lines centered at 16 and 31 cm^{-1} which are absent in the calculated Raman spectrum of α-4T/HT. In addition, we note an inversion of the intensity of the doublet centered around 90 cm^{-1} in the two calculated spectra of α-4T polymorph phases. So, these results show that the transferability of the BP parameters obtained via the BP/$\tilde{\pi}$ model are sufficiently accurate to investigate the polymorphism of α-4T.

B. Raman Intensities in α-6T. To check further the transferability of the α-2T BP/$\tilde{\pi}$ parameters, we also computed the Raman spectrum of the LT phase of α-6T (α-6T/LT)[45] polycrystalline powder. We followed the same strategy as in the previous subsection, using the phonon frequencies and eigenvectors previously computed for α-6T/LT in ref 10.

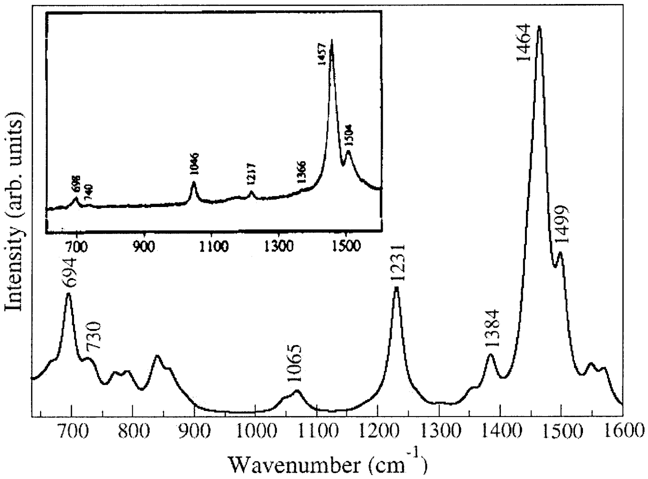

Figure 6. Unpolarized nonresonant Raman spectrum of α-6T/LT calculated for a polycrystalline powder and the experimental one (inset). The experimental spectrum is from ref 12.

The computed Raman spectrum of α-6T/LT displayed in Figure 6 shows a good overall agreement with the experimental one, especially in view of the simplicity of the approach and the absence of any fitting procedure. The intensities of the seven main experimental Raman lines reported on the figure are correctly predicted, except for the two lines between 1000 and 1300 cm^{-1}. Raman lines with small intensities are also theoretically predicted in the 750−850 cm^{-1} range and at 1550 cm^{-1} that are not observed on the experimental spectrum. However, the large scale used in the figure displaying the experimental spectrum does not allow to rule out definitively the existence of these active modes. So, this confirms on another example that the transferability of the α-2T BP/$\tilde{\pi}$ parameters can be considered as a valuable tool to provide reasonable predictions, and at a low computational cost, of the main features of the powder Raman spectra in longer oligothiophenes.

7. Conclusions

In this paper, we have shown that DFT coupled with the nonlinear response formalism allows easy and accurate prediction of the nonresonant Raman spectrum of oligothiophene crystals. In this context, we have proposed, for the first time, an assignment of the main Raman lines of α-2T over the whole frequency range, including the lowest frequencies between 0 and 80 cm^{-1} that are not experimentally available at this time.

Then, we have built a BP model limited to first neighbors both from the fit of $\pi_{ij,\gamma}^{\kappa}$ coefficients and from the direct fit of the experimental Raman spectrum. Although the BP model cannot accurately reproduce the changes of dielectric susceptibility under individual atomic displacements, it was shown to be accurate enough to reproduce the profile of the unpolarized nonresonant Raman powder spectrum of α-2T.

Finally, the transferability of the α-2T BP parameters has also been investigated in longer oligothiophenes. We have observed that only the α-2T BP parameters fitted at a microscopic level are transferable to α-4T and α-6T, whereas those obtained from the global fit of the experimental Raman intensities are not. Our study of α-4T also allowed the Raman signatures of the α-4T/LT and α-4T/HT phases to be identified.

First-principles and BP/$\tilde{\pi}$ approaches appear therefore as efficient complementary tools to calculate the nonresonant Raman spectrum of α-2T and then make reasonable predictions on longer oligothiophenes. The computational strategy proposed in this paper could be tested on other π-conjugated oligomers.

Acknowledgment. The calculations have been performed at CINES (France) and CISM (Université Catholique de Louvain (Belgium), FNRS: project FRFC N °2.4502.05 "Simulation numérique. Application en physique de l′état solide, océanographie et dynamique des fluides"). We thank A. Pasquarello for interesting discussions about the bond polarizability model. This work was supported by the VolkswagenStiftung and the European Network of Excellence FAME.

References and Notes

(1) Fichou, D. *J. Mater. Chem.* **2000**, *10*, 571.

(2) Horowitz, G. *Adv. Mater.* **1998**, *10*, 365.

(3) Katz, H. E. *J. Mater. Chem.* **1990**, *7*, 369.

(4) Schon, J. H.; Dodabalapur, A.; Kloc, Ch.; Batlogg, B. *Science* **2000**, *290*, 963.

(5) Fichou, D. (Ed.) *Handbook of Oligo- and Polythiophenes*; Wiley-VCH: Weinheim, 1999.

(6) Hohenberg, P.; Kohn, W. *Phys. Rev.* **1964**, *136*, B864.

(7) Kohn, W.; Sham, L. J. *Phys. Rev.* **1965**, *140*, A1133.

(8) Degli Esposti, A.; Zerbetto, F. *J. Phys. Chem. A* **1997**, *101*, 7283.

(9) Hermet, P.; Bantignies, J.-L.; Rahmani, A.; Sauvajol, J.-L.; Johnson, M. R. *J. Phys.: Condens. Matter* **2004**, *16*, 7385.

(10) Hermet, P.; Bantignies, J.-L.; Rahmani, A.; Sauvajol, J.-L.; Johnson, M. R. *J. Phys. Chem. A* **2005**, *109*, 4202.

(11) van Eijck, L.; Johnson, M. R.; Kearley, G. *J. Phys. Chem. A* **2003**, *107*, 8980.

(12) Louarn, G.; Buisson, J. P.; Lefrant, S.; Fichou, D. *J. Phys. Chem.* **1995**, *99*, 11399.

(13) Ramírez, F. J.; Hernández, V.; López Navarrete, J. T. *J. Comput. Chem.* **1994**, *15*, 405.

(14) Zerbi, G.; Chierichetti, B.; Ingänas, O. *J. Chem. Phys.* **1991**, *94*, 4637.

(15) Degli Esposti, A.; Moze, O.; Taliani, C.; Tomkinson, J. T.; Zamboni, R.; Zerbetto, F. *J. Chem. Phys.* **1996**, *104*, 9704.

(16) Degli Esposti, A.; Fanti, M.; Muccini, M.; Taliani, C.; Ruani, G. *J. Chem. Phys.* **2000**, *112*, 5957.

(17) Veithen, M.; Gonze, X.; Ghosez, Ph. *Phys. Rev. B* **2005**, *71*, 125107.

(18) Veithen, M.; Gonze, X.; Ghosez, Ph. *Phys. Rev. Lett.* **2004**, *93*, 187401.

(19) Wolkenstein, M. V. *C. R. Acad. Sci. URSS* **1941**, *30*, 741.

(20) Eliashevich, M. A.; Wolkenstein, M. V. *J. Phys. URSS* **1944**, *9*, 101.

(21) Garcia, P.; Pernaut, J.-M.; Hapiot, P.; Wintgens, V.; Valat, P.; Garnier, F.; Delabouglise, D. *J. Phys. Chem.* **1993**, *97*, 513.

(22) De Oliveira, M. A.; Dos Santos, H. F.; De Almeida, W. B. *Phys. Chem. Chem. Phys.* **2000**, *2*, 3373.

(23) Cardona M.; Güntherodt G. *Light Scattering in Solids II*; Springer-Verlag: Berlin, 1982.

(24) Landau, L. D.; Lifshitz, E. M. *Mechanics*; Pergamon Press: Oxford, 1960.

(25) Gonze, X.; Beuken, J.-M.; Caracas, R.; Detraux, F.; Fuchs, M.; Rignanese, G.-M.; Sindic, L.; Verstraete, M.; Zerah, G.; Jollet, F.; Torrent, M.; Roy, A.; Mikami, M.; Ghosez, Ph.; Raty, J.-Y.; Allan, D. C. *Comput. Mater. Sci.* **2002**, *25*, 478.

(26) Pelletier, M.; Brisse, F. *Acta Crystallogr.* **1994**, *C50*, 1942.

(27) Press, W. H.; Flannery, B. P.; Teukolsky, S. A.; Vetterling, W. T. *Numerical recipes (FORTRAN Version)*; Cambridge University Press: Cambridge, 1989.

(28) Perdew, J. P.; Wang, Y. *Phys. Rev. B* **1992**, *45*, 13244.

(29) Ceperley, D. M.; Alder, B. J. *Phys. Rev. Lett.* **1980**, *45*, 566.

(30) Troullier, N.; Martins, J. L. *Phys. Rev. B* **1991**, *43*, 1993.

(31) Fuchs, M.; Scheffler, M. *Comput. Phys. Commun.* **1999**, *119*, 67.

(32) Monkhorst, H. J.; Pack, J. D. *Phys. Rev. B* **1976**, *13*, 5188.

(33) Gonze, X.; Lee, C. *Phys. Rev. B* **1997**, *55*, 10355.

(34) Nunes, R. W.; Gonze, X. *Phys. Rev. B* **2001**, *63*, 155107.

(35) ν = stretching, δ = in-plane bending, γ = out-of-plane bending, *s* = symmetric, *as* = antisymmetric.

(36) Furukawa, Y.; Sakamoto, A.; Ohta, H.; Tasumi, M. *Synth. Met.* **1992**, *49−50*, 335.

(37) Akimoto, M.; Furukawa, Y.; Takeuchi, H.; Harada, I.; Soma, Y.; Soma, M. *Synth. Met.* **1986**, *15*, 353.

(38) Furukawa, Y.; Akimoto, M.; Harada, I. *Synth. Met.* **1987**, *18*, 151.

(39) Anderson, E.; Bai, Z.; Bischof, C.; Blackford, S.; Demmel, J.; Dongarra, J.; Du Croz, J.; Greenbaum, A.; Hammarling, S.; McKenney, A.; Sorensen, D. *LAPACK Users' Guide*, 3rd ed.; Society for Industrial and Applied Mathematics: Philadelphia, 1999.

(40) Umari, P.; Pasquarello, A.; Dal Corso, A. *Phys. Rev. B* **2001**, *63*, 094305.

(41) Loudon, R. *Adv. Phys.* **1964**, *13*, 423.

(42) Siegrist, T.; Kloc, C.; Laudise, R. A.; Katz, H. E.; Haddon, R. C. *Adv. Mater.* **1998**, *10*, 379.

(43) Hermet, P.; Bantignies, J.-L.; Sauvajol, J.-L.; Johnson, M. R. *Synth. Met.* **2006**, *156*, 519.

(44) Parlinski, K. *Am. Inst. Phys. Conf. Proc.* **1999**, *479*, 121.

(45) Horowitz, G.; Bachet, B.; Abderrahim, Y.; Lang, P.; Demanze, F.; Fave, J.-L.; Garnier, F. *Chem. Mater.* **1995**, *7*, 1337.

(46) Siegrist, T.; Fleming, R. M.; Haddon, R. C.; Laudise, R. A.; Lovinger, A. J.; Katz, H. E.; Bridenbaugh, P.; Davis, D. D. *J. Mater. Res.* **1995**, *10*, 2170.